China Geology 6 (2023) 228−240

China Geology

Journal homepage: http://chinageology.cgs.cn
https://www.sciencedirect.com/journal/china-geology

Potential seismic landslide hazard and engineering effect in the Ya'an-Linzhi section of the Sichuan-Tibet transportation corridor, China

Zhi-hua Yang[a, b, c], Chang-bao Guo[a, b,*], Rui-an Wu[a, b], Wei-wei Shao[a, d], Peng-fei Yu[a, e], Cai-hong Li[a, e]

[a] *Institute of Geomechanics, Chinese Academy of Geological Sciences, Beijing* 100081, *China*
[b] *Key Laboratory of Active Tectonics and Geological Safety, Ministry of Natural Resources, Beijing* 100081, *China*
[c] *State Key Laboratory of Resources and Environmental Information System, Beijing* 100101, *China*
[d] *China University of Geosciences, Wuhan* 430074, *China*
[e] *China University of Geosciences (Beijing), Beijing* 100083, *China*

ARTICLE INFO

Article history:
Received 17 December 2022
Received in revised form 13 February 2023
Accepted 23 March 2023
Available online 3 April 2023

Keywords:
Qinghai-Tibet Plateau
Sichuan-Tibet transportation corridor
Seismic landslide
Hazard assessment
Engineering effect

ABSTRACT

The Sichuan-Tibet transportation corridor is located at the eastern margin of the Qinghai-Tibet Plateau, where the complex topography and geological conditions, developed geo-hazards have severely restricted the planning and construction of major projects. For the long-term prevention and early control of regional seismic landslides, based on analyzing seismic landslide characteristics, the Newmark model was used to carry out the potential seismic landslide hazard assessment with a 50-year beyond probability 10%. The results show that the high seismic landslide hazard is mainly distributed along large active tectonic belts and deep-cut river canyons, and are significantly affected by the active tectonics. The low seismic landslide hazard is mainly distributed in the flat terrain such as the Quaternary basins, broad river valleys, and plateau planation planes. The major east-west linear projects mainly pass through five areas with high seismic landslide hazard: Luding-Kangding section, Yajiang-Xinlong (Yalong river) section, Batang-Baiyu (Jinsha river) section, Basu (Nujiang river) section, and Bomi-Linzhi (eastern Himalaya syntaxis) section. The seismic action of the Bomi-Linzhi section can also induce high-risk geo-hazard chains such as the high-level glacial lake breaks and glacial debris flows. The early prevention of seismic landslides should be strengthened in the areas with high seismic landslide hazard.

1. Introduction

The Qinghai-Tibet Plateau is a special region with the most intense tectonic activities in China and even in the world, where there are the complex landforms and geological structures, developed active faults. The frequent historical earthquakes have induced a large number of secondary geo-hazard chains such as landslides, dammed rivers and barrier lakes, so the risk of seismic geo-hazards is high (Peng C et al., 2021). In recent years, there have been many strong earthquakes on the Qinghai-Tibet Plateau. The huge M_S 8.0 Wenchuan earthquake in 2008 triggered a large number of secondary geo-hazards, which posed a serious threat to the safety of residents and major projects in the seismic area (Yin YP et al., 2011; Dai FC et al., 2011; Yin YP, 2014; Tang HM et al., 2015). After the Wenchuan earthquake, the M_S 7.0 Lushan earthquake in 2013 (Zhang YS et al., 2013), M_S 6.5 Ludian earthquake in 2014, M_S 6.3 Kangding earthquake in 2014 and M_S 6.8 Luding earthquake on September 5, 2022 successively occurred. A large number of loose deposits caused by earthquakes provide abundant material sources for subsequent geo-hazards, which are easy to be transformed into geo-hazards again under the post-earthquake rainfall effect. So, the seismic effect can significantly increase the susceptibility and intensity of subsequent geo-hazards.

Seismic landslide hazard has attracted extensive attention in the geo-hazard research field. Abundant research works on seismic landslides have been carried out, and some effective and sophisticated methods and models have been established to complete the seismic landslide susceptibility and hazard assessment, such as multi-criterion evaluation method (Kamp U et al., 2008), artificial neural network (ANN) (Lee S and

First author: *E-mail address*: yangzh99@163.com (Zhi-hua Yang).
* Corresponding author: *E-mail address*: guochangbao@163.com (Chang-bao Guo).

Literary editor: Jie Meng
doi:10.31035/cg2023032
2096-5192/© 2023 China Geology Editorial Office.

Evangelista DG, 2006), support vector machine (SVM) (Xu C et al., 2012), Bayesian network (Song YQ et al., 2012), and logistic regression (Nefeslioglu HA et al., 2006). For considering the physical meaning and seismic dynamic effect on slope masses failure, the Newmark model (Miles SB and Ho CL, 1999; Wilson RC and Keefer DK, 1983) and related empirical predictive models (Chousianitis K et al., 2014) and statistical probabilistic models (Nowicki MA et al., 2014) have been established to carry out seismic slope displacement simulation and landslide hazard assessment.

With the implementation of China's western development and poverty alleviation strategy, major projects and urban construction such as railways, highways, hydropower stations, water transmission lines and trans-regional power grids on the Qinghai-Tibet Plateau are developing rapidly, which are bound to face serious threats from potential seismic landslides in the areas with active faults. The Sichuan-Tibet transportation corridor is located at the eastern margin of the Qinghai-Tibet Plateau, which has the largest topographic steepness, the strongest internal and external dynamic geological action, and the extremely frequent geo-hazards, and it is the first step of the land topography in China. Where, a lot of research results on landslide susceptibility and hazard assessment have been completed (Wu RA et al., 2020). But, the research results on seismic landslide assessment are relative lacking, and most of them are mainly for local areas (such as active fault zones) (Xu C et al., 2012; Zhang YS et al., 2017) or single earthquake event (such as the Wenchuan earthquake in 2008 and Lushan earthquake in 2013) (Wang T et al., 2013; Yang ZH et al., 2015). The research on potential seismic landslide of the whole line of Sichuan-Tibet transportation corridor needs to be strengthened and its impact on major projects should be considered.

Considering the regional seismic geological setting, seismic activity characteristics, long-term seismic landslide prevention and control necessary of major projects and urban planning and construction, and on the basis of analyzing regional topography, geological structure, stratigraphic lithology and typical seismic landslides, the Newmark model based on general statistical law (Newmark NM, 1965; Jibson RW et al., 2000; Roberto R, 2000) was adopted to carry out the prediction and assessment of potential seismic landslide hazard in the Ya'an-Linzhi section of Sichuan-Tibet transportation corridor, which initially reflected the spatial distribution characteristics of regional seismic landslide hazard, and analyzed its influence on the engineering planning and construction. The study results can provide scientific reference for the long-term prevention and control of seismic landslides of major projects in the Sichuan-Tibet transportation corridor.

2. Seismic geological settings

The Sichuan-Tibet transportation corridor is located at the eastern margin of the Qinghai-Tibet Plateau, starting from Chengdu city of Sichuan province in the east and reaching Lasa city of Tibet in the west. It rises from the Sichuan Basin on the second step to the Qinghai-Tibet Plateau on the first step of land topography in China, where the landform is dominated by the plateau basins and deep valleys. The Sichuan-Tibet transportation corridor spans 16 major rivers, including the Dadu river, Yalong river, Jinsha river, Lancang river, Nujiang river and Yarlung Zangbo river, and passes through 21 snow-capped mountains, including Hengduan Mountain Range, Taniantaweng Mountain Range and Nianqing Tanggula Mountain Range, with extremely complex landforms and geological settings. The strata are well developed, and the geological structure has a significant controlling effect on the strata distribution, such as the strata strike is basically consistent with the regional fault strike (Fig. 1). Except for the Cambrian, the strata are distributed from the Quaternary to the Sinian, and the sedimentary rocks are the main ones.

Since the Late Cenozoic, the neotectonic movement of the Qinghai-Tibet Plateau has been intense, and the Sichuan-Tibet transportation corridor traverses the Yangtze Block, Sichuan-Yunnan Block, Gansu-Qinghai Block, Tibet Block and Himalayan Block from east to west (Deng QD et al., 1996). During Quaternary, the subduction and extrusion of the Indian plate into the Eurasian plate resulted in the rapid uplift of the Qinghai-Tibet Plateau at a speed of 9.5 mm/a (Tapponnier P and Molnar P, 1977), which then resulted in strong modern crustal activity and high crustal stress field (Zhu SB and Shi YL, 2005; Meng W et al., 2022). As a further result, the active fault zones with different directions were formed in the parts of uneven crustal movement, such as the Longmenshan fault zone, Xianshuihe fault zone, Litang-Dewu fault zone, Jinshajiang fault zone, Lancangjiang fault zone, Nujiang fault zone, Chayu-Jiali fault zone, etc. (Fig. 2). According to the *Seismic Ground Motion Parameters Zonation Map of China* (GB 18306-2015) issued by the China Earthquake Administration, the peak ground motion acceleration of Sichuan-Tibet transportation corridor is all greater than or equal to 0.10 g (seismic fortification intensity ⩾7 degrees), and the corridor with the peak ground motion acceleration of 0.2 g or above are about 500 km long, accounting for 52% of the total length. The peak ground motion acceleration in the southern Luding-Kangding section of the Xianshuihe fault zone is up to 0.4 g, and the peak ground motion acceleration in the Bomi-Linzhi section on the northern side of the great bend of the Yarlung Zangbo river is up to 0.3 g. In history, there have been many strong earthquakes that have caused heavy casualties, such as the M_S 8.6 Chayu earthquake in 1950, the M_S $7^3/_4$ Kangding earthquake in 1786, the M_S 6.7 Batang earthquake in 1989, and the M_S 8.0 Wenchuan earthquake in 2008.

3. Seismic landslide development characteristics

The Sichuan-Tibet transportation corridor runs through the Hengduan Mountain Range, with high mountains and deep valleys, and strong topography cutting and rock fragmentation. The shallow surface geo-hazards such as

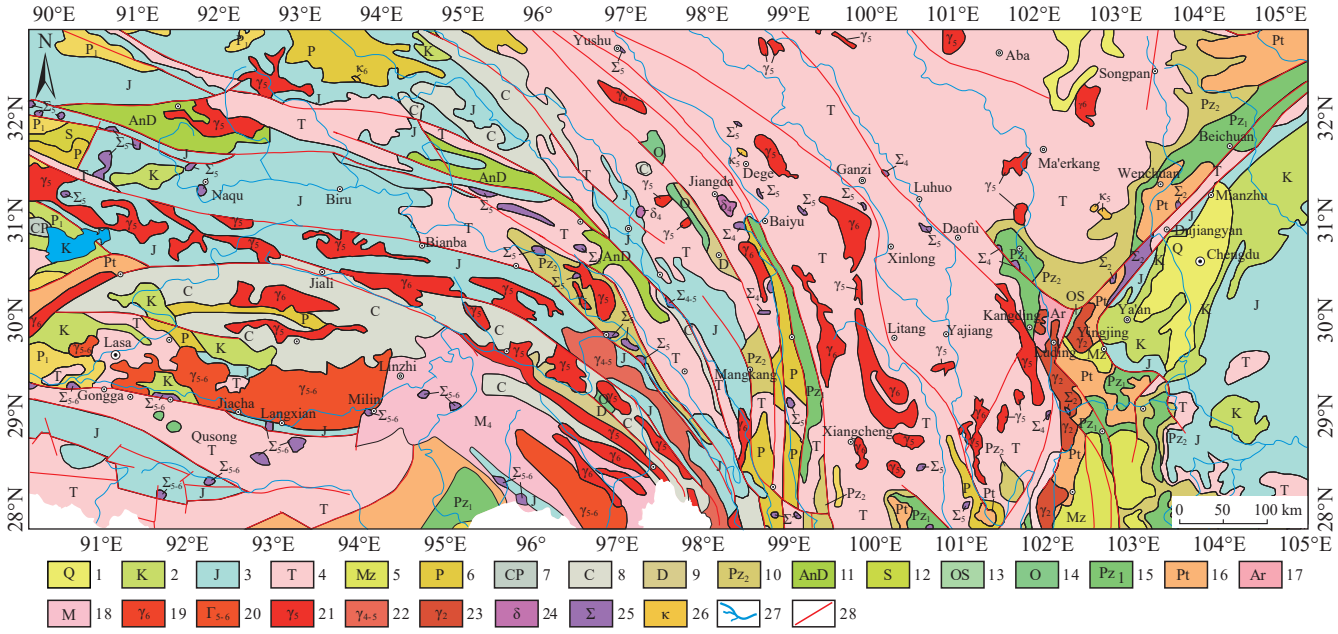

Fig. 1. Geological settings of the Sichuan-Tibet transportation corridor (the simplified geological data comes from the regional geological maps with 1∶200000 scale).1–Quaternary alluvium, moraine, etc.; 2–terrestrial clastic rocks, marine clastic rocks and volcanic rocks; 3–terrestrial clastic rocks, marine sedimentary rocks in the South Tibet (sand-shale mixed with marl); 4–marine sand slate mixed with limestone, sand-shale, conglomerate and volcanic rocks; 5–Mesozoic stratification; 6–Gondwana facies (limestone, sand-slate mixed with basalt and phyllite); 7–mixed stratum; 8–Gondwana facies (sand-shale, marble and limestone); 9–molarite of middle-upper Devonian; 10–mixed stratum of upper Paleozoic; 11–Pre-Devonian metamorphic sand-slate, gneiss and marble; 12–limestone mixed with phyllite, marble mixed with mafic volcanic rocks; 13–mixed stratum; 14–clastic rocks and volcanic rocks; 15–mixed stratum of lower Paleozoic; 16–Proterozoic; 17–Archean; 18–Mesozoic mixtite; 19–Himalayan granite; 20–Late Yanshanian-Himalayan granite; 21–Yanshanian granite; 22–Hualisian-Yanshanian granite; 23–Proterozoic granite; 24–diorite type; 25–ultramafic rocks; 26–alkaline rocks; 27–drainage; 28–faults.

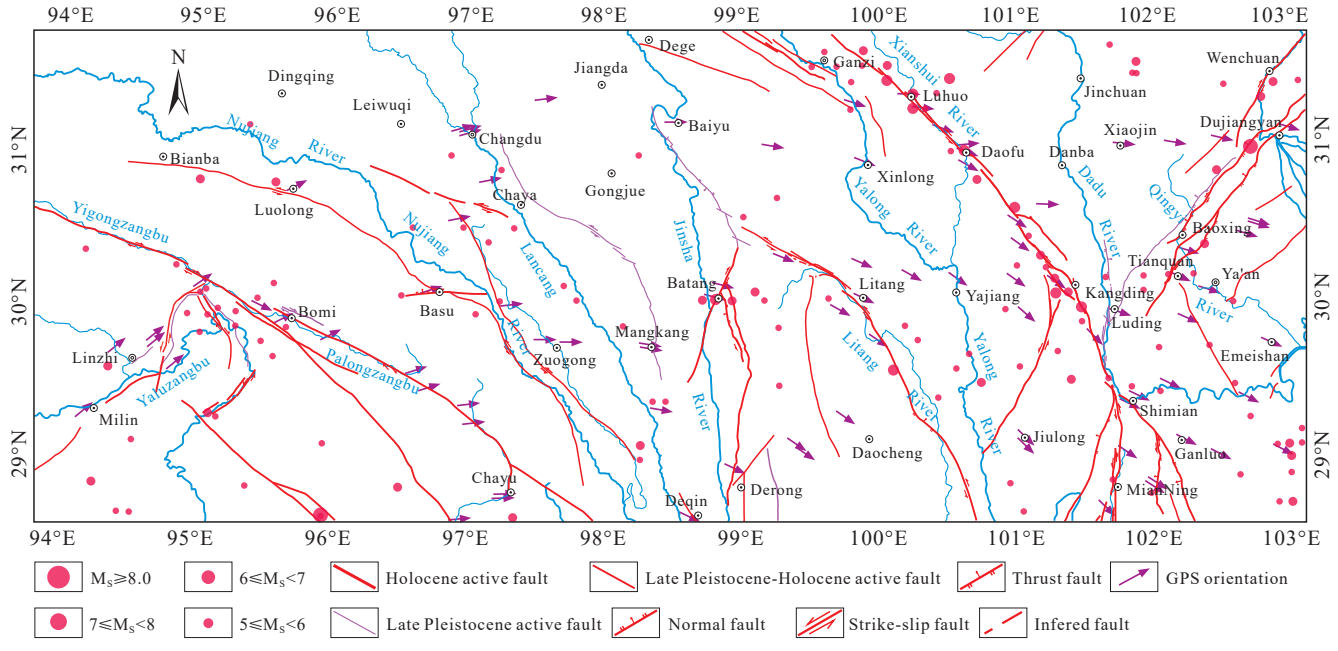

Fig. 2. Active faults and historical earthquakes in the Ya'an-Linzhi section of the Sichuan-Tibet transportation corridor (the simplified faults come from the regional geological maps with 1∶200000 scale and the earthquake epicenter data come from the China Earthquake Administration).

collapse, landslide and debris flow formed under the internal and external dynamic coupling action are characterized by a wide distribution area, large scale, great harm, frequent recurrence and complex formation mechanism (Fig. 3; Delaney KB and Evans SG, 2015; Guo CB et al., 2020). The geo-hazard data in Fig. 3 come from the county geo-hazard survey database organized by the Ministry of Natural Resources of China and the field survey of huge and typical geo-hazard along and around major projects. And, the large-scale geo-hazards are selected to calculate the geo-hazard

density, which is more representative of the harm from geo-hazards. The geo-hazards shown in the Fig. 3 are typical and representative super-large-scale landslides, collapses, and debris flows, such as the Luanshibao landslide, Yigong landslide and Baige landslide. The landslides in the Sichuan-Tibet corridor are significantly affected by the regional tectonics and active faults, and their sliding direction is mostly perpendicular to the fault strike and the flow direction of rivers.

Earthquake is an important internal dynamic geological factor to induce geo-hazards. Strong earthquakes may not only form large scale surface rupture zones, but also destroy the intrinsic stability of natural slopes, thus forming large-scale geo-hazards. The seismic landslide is affected by the throwing force, which starts fast and has large potential energy and long runout, and may cause "catastrophe" at the slope foot or transform into a destructive geo-hazard chain. The Sichuan-Tibet transportation corridor passes through many Holocene active faults, such as Longmenshan fault zone, Xianshuihe fault zone and Batang fault zone, and a large number of catastrophic earthquake-induced landslide events have occurred in the history. In 1973, the M_S 7.9 Luhuo earthquake in the Xianshuihe fault zone triggered more than 160 landslides, and the linear landslide distribution characteristics along the fault were very prominent (Li MH et al., 2014). In 1786, the Mogangling landslide in Luding county induced by the M_S $7^3/_4$ Kangding earthquake blocked Dadu river and formed huge barrier lake. In 1950, the M_S 8.6 Chayu earthquake in Tibet induced a large number of avalanche, ice collapse, rockfall and landslide disasters, and accumulated a large number of loose accumulation materials in the long and steep Guxiang gully of Bomi county, which seriously increased the development intensity and frequency of debris flow in the Guxiang gully. By means of field investigation and geological dating, several large-scale paleo-seismic landslides with a scale of one thousand years have been found (Fig. 4), such as the Luanshibao landslide with high location and long runout in the margin of Maoyaba basin of Litang county (Guo CB et al., 2016), Temi landslide blocking Jinsha river in Batang county, Langduo landslide group in Batang county, etc.

In recent years, there have been frequent earthquake events in the Sichuan-Tibet transportation corridor. The M_S 8.0 Wenchuan earthquake in 2008 induced tens of thousands of geo-hazards, which were the most densely distributed, the largest scale and the most serious catastrophe recorded so far (Yin YP et al., 2011; Yin YP, 2014), and significantly increased the earthquake-induced losses. The M_S 7.0 Lushan earthquake in 2013 (Zhang YS et al., 2013; Yang ZH et al., 2015; Shao XY et al., 2022), M_S 6.5 Ludian earthquake in 2014, M_S 6.3 Kangding earthquake in 2014 and other strong earthquakes induced many landslide disasters. On September 5, 2022, one M_S 6.8 earthquake occurred in Luding county, Sichuan province, which triggered many secondary avalanches and landslides (Fig. 5). The Luding earthquake-induced landslides are mainly small and medium-sized, and the large and giant landslides are relatively less, and some landslides with high location are transformed into landslide-debris flow disaster chains (Fan XM et al., 2022; Huang YD et al., 2022).

4. Seismic landslide hazard assessment

The research on the seismic landslide hazard has gradually developed from qualitative to semi-quantitative and quantitative, and the presented models and methods are becoming more and more abundant. The Newmark model predicts seismic landslide hazard by calculating the accumulated slope displacement under seismic load (Newmark NM, 1965), and has been widely used (Jibson RW et al., 2000; Zhang YS et al., 2017). In this paper, on the basis of considering the regional seismic geological settings, the Newmark model is used to carry out the potential seismic

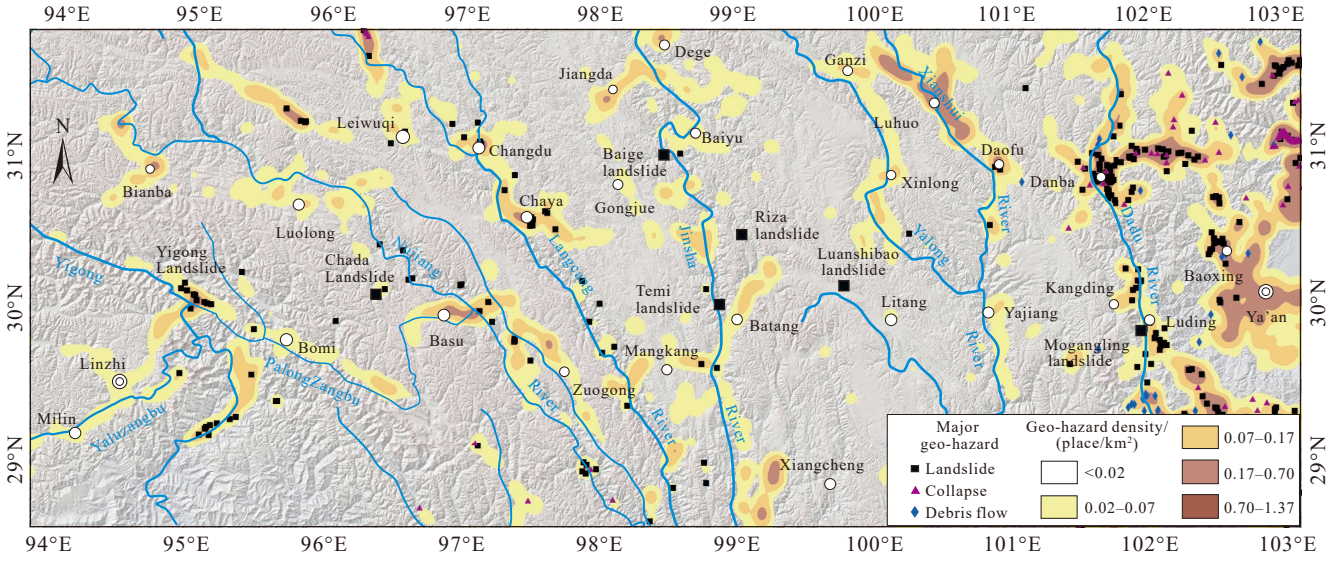

Fig. 3. Major geo-hazard distribution in the Ya'an-Linzhi section of the Sichuan-Tibet transportation corridor.

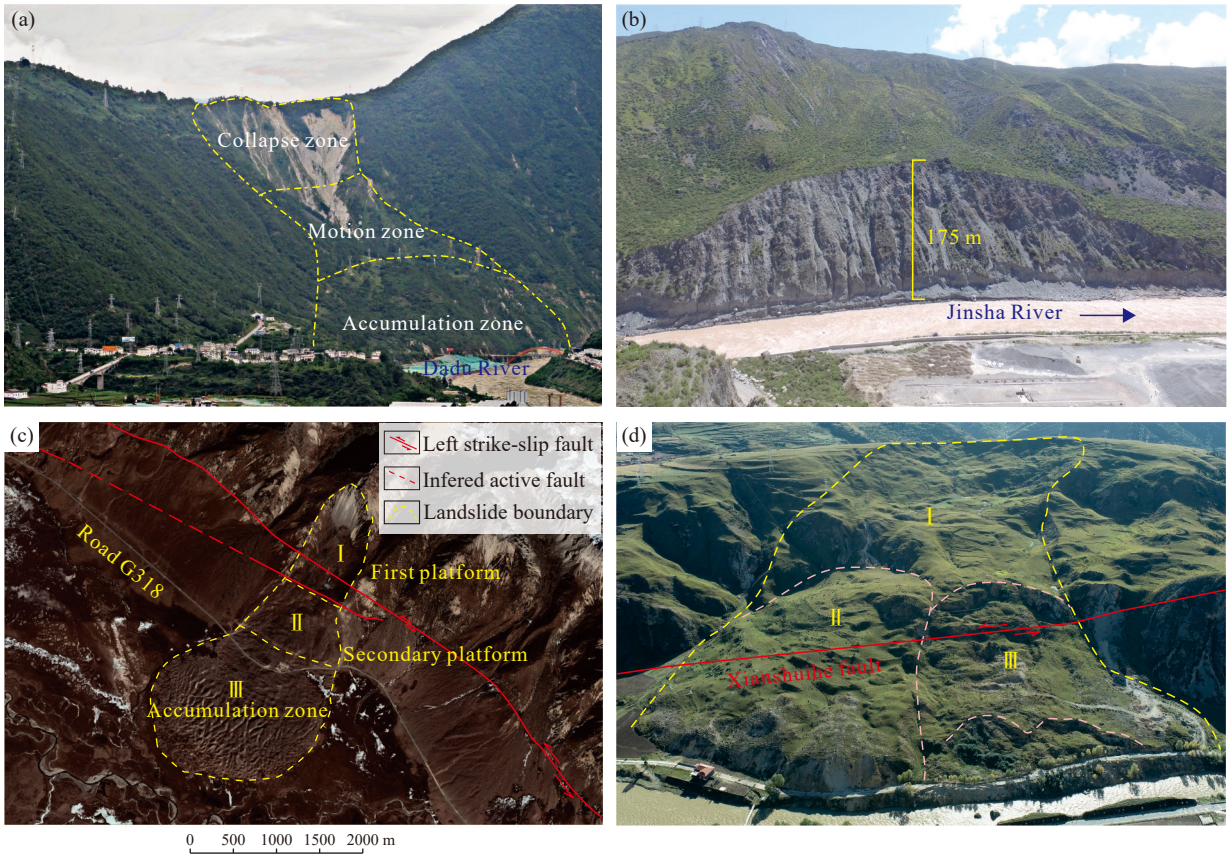

Fig. 4. Seismic landslides characteristics in the Ya'an-Linzhi section of the Sichuan-Tibet transportation corridor.a–Mogangling landslide in the Luding county; b–Temi landslide in the Batang county; c–Luanshibao landslide in the Litang county; d–55 Daoban landslide in the Luhuo county.

landslide hazard assessment of the Ya'an-Linzhi section of the Sichuan-Tibet transportation corridor.

4.1. Newmark model principle and calculation process

The theoretical basis of the Newmark model is the limit equilibrium theory of infinite slope. This model regards the sliding body as a rigid body, and mainly studies the critical acceleration and safety factor of the slope itself. When the acceleration coming from external force is greater than the critical acceleration, a limited displacement of sliding body will occur, and the limited displacement is accumulated continuously to produce permanent displacement of the sliding block (Newmark NM, 1965). The permanent displacement of the sliding body can be obtained by twice integrating the difference between the external load acceleration and the critical acceleration with respect to time (Newmark NM, 1965; Jibson RW, 1993; Jibson RW et al., 2000; Roberto R, 2000).

Based on the statistical analytical results of a large number of seismic landslides, a simplified Newmark calculation model based on statistical laws between seismic landslide hazard and geological parameters was developed (Miles SB and Ho CL, 1999; Jibson RW et al., 2000). Here, the potential seismic parameters are the peak ground motion acceleration under probabilistic seismic conditions. The calculation steps of the seismic landslide hazard are as follows: (1) Based on the regional geological settings, the appropriate parameters of rock and soil mass strength and slope shape are selected to calculate the regional slope static safety factor (F_s); (2) The slope critical acceleration (a_c) is calculated by F_s and slope shape parameters; (3) The permanent slope sliding displacement (D_n) under probabilistic seismic effect is calculated using a_c and peak seismic ground acceleration (PGA); (4) Finally, according to the statistical law of slope displacement and landslide occurrence probability, seismic landslide hazard can be predicted and assessed (Wang T et al., 2013; Zhang YS et al., 2017).

4.2. Seismic landslide hazard assessment

The ArcGIS platform was used to realize the potential seismic landslide hazard assessment based on the Newmark model. The geological data comes from the regional geological maps with 1∶200000 scale, and the engineering geological units can be divided according to the stratum lithology and rock mass structure. The used terrain data comes from the advanced spaceborne thermal emission and reflection radiometer global digital elevation model (ASTER GDEM) with a resolution of 30 m, from which the terrain slope can be generated. The ground motion parameters were based on the fifth-generation seismic ground motion parameters zonation map of China. The resolution of raster

data during calculation was 30 m, and the vector data was converted to raster data to participate in calculation.

4.2.1. Slope static safety factor

The slope static safety factor can represent the slope body stability without the influence of internal and external dynamic disturbances such as earthquake and rainfall. The slope stability factor formula (Eq. 1) based on the limit equilibrium theory was used to calculate the static safety factor (F_s) of the regional slope (Miles SB and Ho CL, 1999; Jibson RW et al., 2000). Among them, c' is the effective internal cohesion of rock-soil masses (kPa), φ' is the effective internal friction angle of rock-soil masses (°), γ is the weight of rock-soil masses (kN/m^3), γ_w is the weight of groundwater (kN/m^3), t is the thickness of potential sliding rock-soil masses (m), α is the inclination angle of potential sliding surface (°), and m is the thickness ratio of saturated part in the total potential sliding rock-soil masses.

$$F_s = \frac{c'}{\gamma t \sin\alpha} + \frac{\tan\varphi'}{\tan\alpha} - \frac{m\gamma_w \tan\varphi'}{\gamma \tan\alpha} = \frac{c'}{\gamma t \sin\alpha} + (1 - \frac{m\gamma_w}{\gamma}) \times \frac{\tan\varphi'}{\tan\alpha} \quad (1)$$

The stratigraphic lithology in the Ya'an-Linzhi section of the Sichuan-Tibet transportation corridor is divided into 13 engineering geological units by comprehensively considering several factors such as geological tectonics, stratigraphic age, rock-soil mass type, and weathering and fragmentation degree of rock masses (Fig. 6, Table 1). According to the *Engineering geology handbook (The fifth edition) of China* (Hua JX et al., 2018), rock-soil masses experiments, literature and expert experience, the physical and mechanical properties of engineering geological units were initialized comprehensively. Then, Equation 1 was used to calculate the slope static safety factor (F_s). During the multiple iterative calculation process, the model parameters were adjusted to ensure that the slope static safety factor (F_s) without internal and external dynamic loading was greater than 1. The model parameters are determined as follows: c', φ' and γ are shown in Table 1, γ_w=10 kN/m^3, t=2.5 m, m=0.3, α is the terrain slope, which comes from the field geological survey knowledge, existing reference literature (Kamp U et al., 2008; Zhang YS et al., 2017; Du GL et al., 2022) and experience understanding. Finally, the slope static safety factor (F_s) of the Ya'an-Linzhi section of the Sichuan-Tibet transportation corridor can be calculated, which is shown in Fig. 7. The regions with lower slope static safety factor (F_s) are more prone to landslide occurrence.

4.2.2. Slope critical acceleration

The slope critical acceleration (a_c) refers to the ground motion acceleration when the sliding force of the sliding masses is equal to the anti-sliding force (limit equilibrium state), which can represent the slope instability potential due to its inherent properties under external seismic motion. By comparing the force state of the sliding masses under static and seismic dynamic conditions, the limit equilibrium equation of the sliding masses was established, and the calculation formula (Eq. 2) of the slope critical acceleration (a_c) was derived (Wilson RC and Keefer DK, 1983). Where, g is the gravity acceleration (m/s^2), and α is the inclination angle of potential sliding surface (°). Then, the slope critical

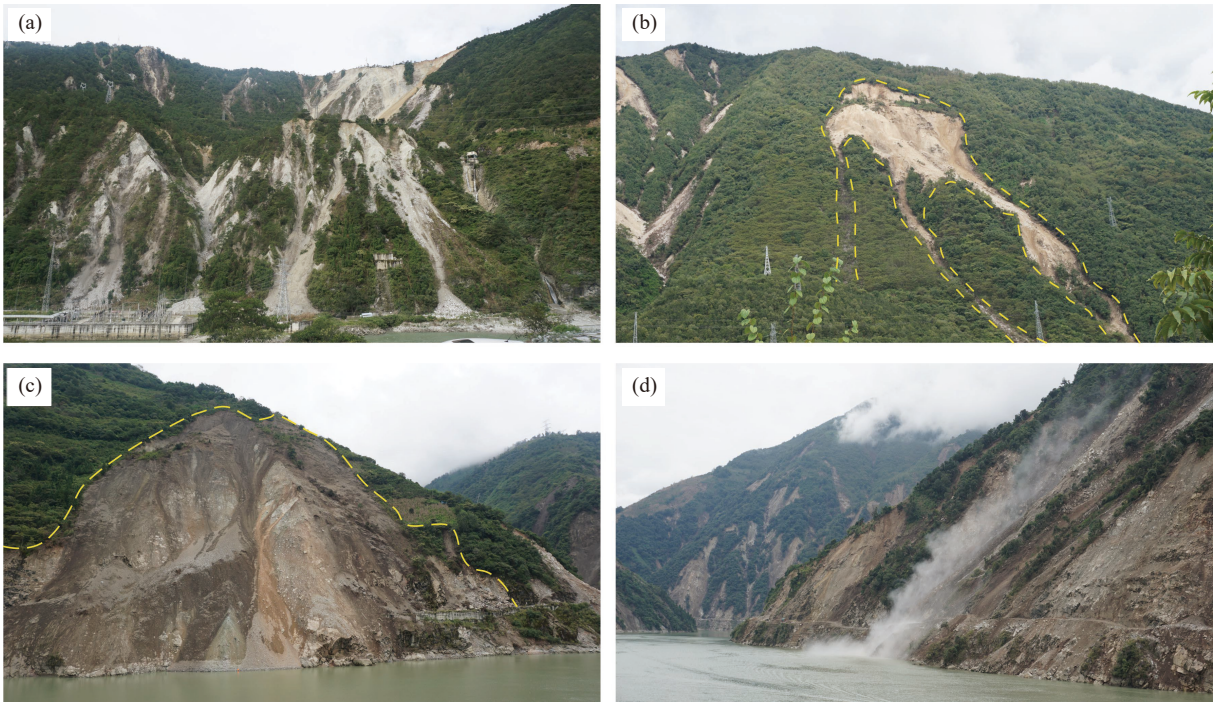

Fig. 5. Landslide characteristics induced by the M_S 6.8 Luding earthquake in the Sichuan province in 2022. a–Deformation and failure of the Mogangling landslide accumulation body; b–landslide and debris flow in the Yanzi gully; c–Xinhuancun landslide in the Detuo town; d–S211 crossroad landslide in the Detuo town.

acceleration (a_c) of the Ya'an-Linzhi section of the Sichuan-Tibet transportation corridor was calculated, which was shown in Fig. 8. The regions with little slope critical acceleration (a_c) are more prone to landslide occurrence with internal and external dynamic effects.

$$a_c = (F_s - 1)g\sin\alpha \tag{2}$$

4.2.3. Seismic slope displacement

In the study area, the rugged topography has a serious amplification effect on the ground seismic motion. The topographic amplification effect for a local prominent terrain can be calculated by Eq. 3 (The Ministry of Construction of the People's Republic of China, 2010; Wang T et al., 2018; Li C and Su LJ, 2021). Where, λ is the topographic amplification coefficient, and α is the increment amplitude of the ground seismic motion, and ξ is the adjustment coefficient. The parameter α was approximately calculated by the slope height and slope gradient (Table 2), and ξ was set to 1 for simplicity (Wang T et al., 2018; Li C and Su LJ, 2021). The slope height and slope gradient can be obtained from DEM data using ArcGIS platform. The fifth-generation seismic ground motion parameters in China (Fig. 9) with a 50-year exceedance probability of 10% was adjusted by Eq. 3. The statistical functional relationship between the seismic slope cumulative displacement (D_n), slope critical acceleration (a_c), and peak seismic ground acceleration intensity (PGA) is shown in Eq. 4 (Jibson RW, 2007). Among them, the slope cumulative displacement (D_n) is positively correlated with the peak

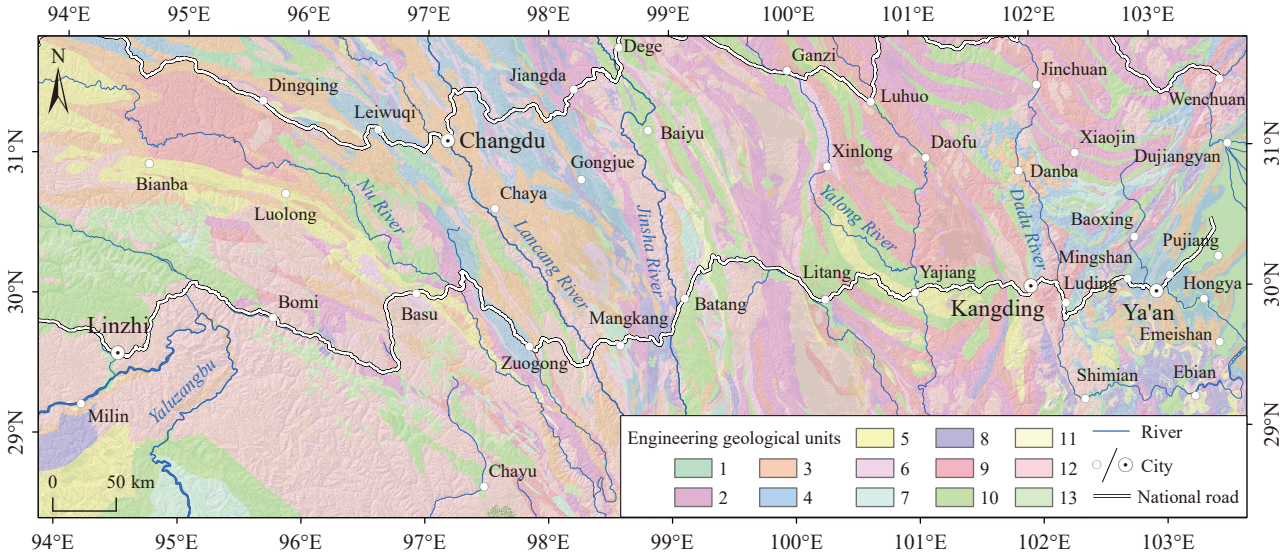

Fig. 6. Engineering geological units in the Ya'an-Linzhi section of the Sichuan-Tibet transportation corridor.

Table 1. Physical and mechanical properties of engineering geological units in the Ya'an-Linzhi section of the Sichuan-Tibet transportation corridor.

ID	Engineering geological units	c'/kPa	φ'/°	γ/(kN/m^3)
1	Hard thick-bedded sandstone	26	33	26
2	Relatively hard to hard medium-thick-bedded sandstone interbedded with conglomerate, mudstone and slate	25	32	25
3	Alternate of soft and hard medium-thick-bedded sandstone and mudstone interbedded with limestone	23	30	24
4	Soft to relatively hard and thin to medium-thick-bedded sandstone and mudstone	22	28	23
5	Soft thin-bedded mudstone and shale	20	27	21
6	Hard medium-thick-bedded limestone and dolomite	24	31	25
7	Relatively hard and thin to medium-thick-bedded limestone and argillaceous limestone	23	30	24
8	Alternate of soft and hard medium-thick-bedded limestone and dolomite interbedded with sandstone and mudstone	22	29	23
9	Relatively hard to hard and thin to medium-thick-bedded slate, phyllite and metamorphic sandstone	21	28	22
10	Soft to relatively hard and thin to medium-thick-bedded phyllite and schist interbedded limestone, sandstone and volcanic rocks.	20	26	21
11	Hard blocky basalt	27	34	29
12	Hard blocky granite, andesite and diorite	26	33	28
13	Soft loose sediments and deposits	15	25	18

ID is the corresponding number of engineering geological units in Fig. 6, c' is the effective internal cohesion, φ' is the effective internal friction angle, and γ is the weight of rock masses.

seismic ground acceleration intensity (PGA), and negatively correlated with the slope critical acceleration (a_c). The adjusted PGA results were used to calculate the seismic slope displacement (D_n) of the Ya'an-Linzhi section of the Sichuan-Tibet transportation corridor, which was shown in Fig. 10. The regions with large slope displacement (D_n) can show high seismic landslide hazard.

$$\lambda = 1 + \xi \times \alpha \tag{3}$$

$$\lg D_n = 0.215 + \log\left[\left(1 - \frac{a_c}{PGA}\right)^{2.341}\left(\frac{a_\varepsilon}{PGA}\right)^{-1.438}\right] \tag{4}$$

4.2.4. Seismic landslide hazard

The slope displacement does not necessarily indicate that significant landslide disasters will definitely occur. Only when the slope displacement has accumulated to a certain extent, the slope will become unstable and slide along the sliding surface, which results in the bothersome landslide disasters. According to extensive experience and research results, there is a statistical relationship between slope displacement and seismic landslide occurrence probability (Jibson RW et al., 2000). Through analyzing the historical landslide data of the M_S 7.9 Luhuo earthquake in 1973 in the Xianshuihe fault zone, a statistical function relationship (Eq. 5) between slope displacement and seismic landslide occurrence probability was established, which is suitable for the active tectonic zone on the eastern margin of the Qinghai-Tibet Plateau (Zhang YS et al., 2017). This equation was used to calculate the landslide occurrence probability index (p) under the potential seismic dynamic actions in the Ya'an-Linzhi section of the Sichuan-Tibet transportation corridor. And, the higher the index, the greater the seismic landslide hazard.

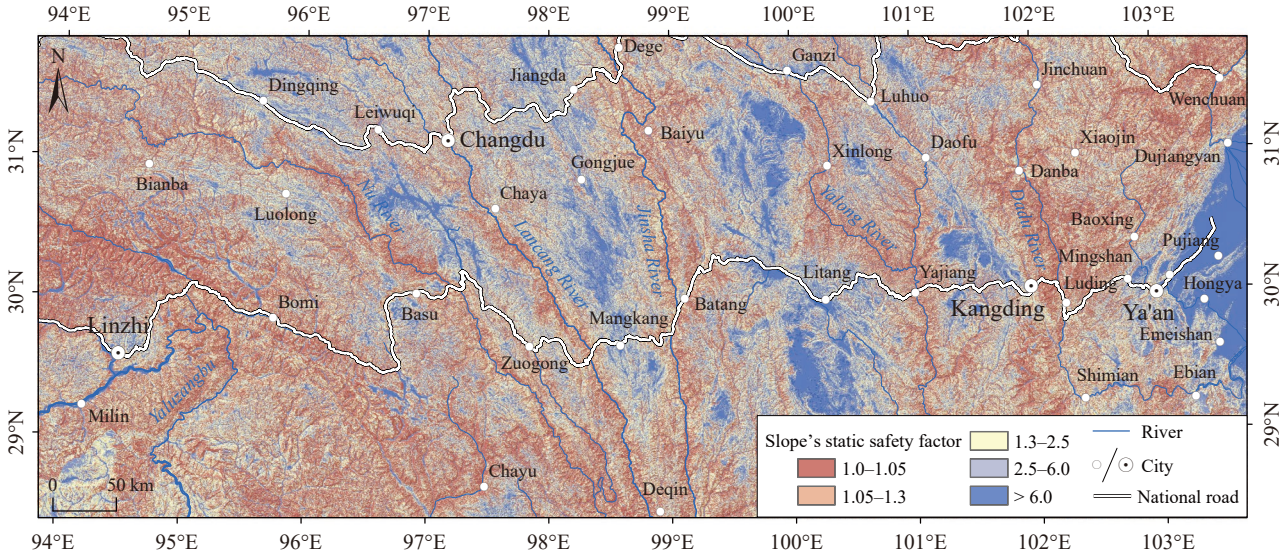

Fig. 7. Slope static safety factor in the Ya'an-Linzhi section of the Sichuan-Tibet transportation corridor.

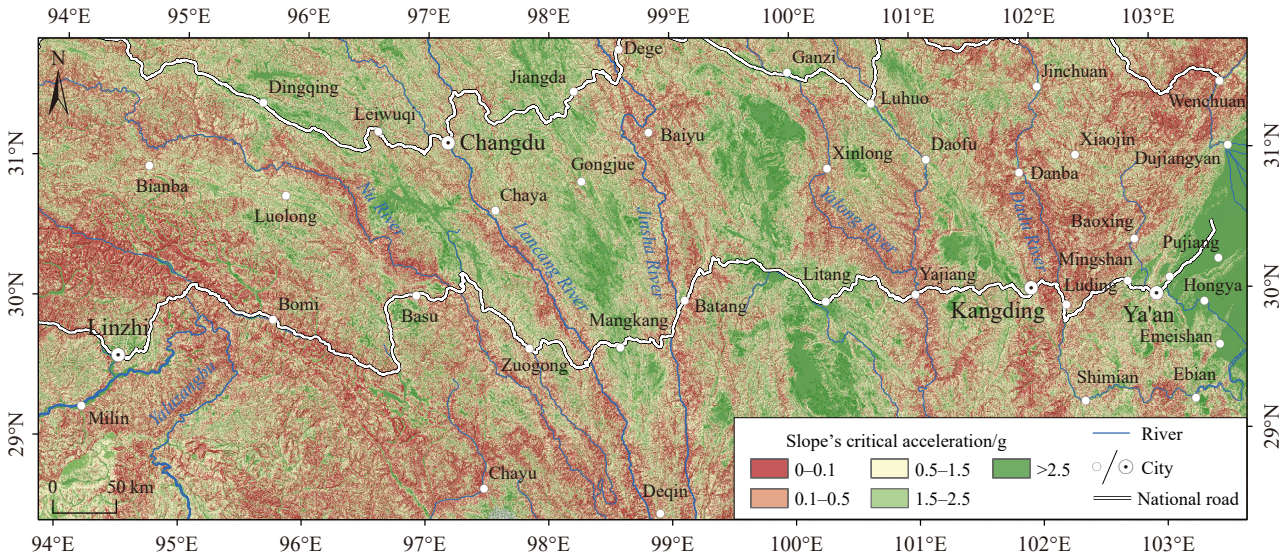

Fig. 8. Slope critical acceleration in the Ya'an-Linzhi section of the Sichuan-Tibet transportation corridor.

$$P = 0.238\left[1-\exp(-0.0034D_n^{2.4354})\right] \quad (5)$$

5. Seismic landslide hazard results and engineering effect

5.1. Distribution characteristics of seismic landslide hazard

According to the seismic landslide occurrence probability index, combined with the regional seismic geological settings and the field seismic landslide survey, the potential seismic landslide hazard in the Ya'an-Linzhi section of the Sichuan-Tibet transportation corridor can be divided into three levels (Fig. 11) as follows: low seismic landslide hazard (seismic landslide occurrence probability is less than 5%), accounting for about 62.41% of the total area; medium seismic landslide hazard (seismic landslide occurrence probability is 5%–15%), accounting for about 24.43% of the total area; high seismic landslide hazard (seismic landslide occurrence probability is more than 15%), accounting for about 13.16% of the total area. In general, the areas with high seismic landslide hazard are distributed in a zonal pattern approximately from south to north, and are mainly distributed along large active tectonic belts and deep valleys of large rivers. They are significantly affected by tectonic activities, especially the "Y" active tectonic zone in the east and the eastern Himalaya syntaxis in the west,

Table 2. The empirical increment parameters of the topographic amplification effect (Wang T et al., 2018; Li C and Su LJ, 2021).

H	Soil slope	*H*<5	5⩽*H*<15	15⩽*H*<25	*H*⩾25
	Rock slope	*H*<20	20⩽*H*<40	40⩽*H*<60	*H*⩾60
H/L	*H/L*<0.3	0	0.1	0.2	0.3
	0.3⩽*H/L* <0.6	0.1	0.2	0.3	0.4
	0.6⩽*H/L* <1.0	0.2	0.3	0.4	0.5
	H/L⩾1.0	0.3	0.4	0.5	0.6

Note: H represents the slope height and H/L represents the slope tangent.

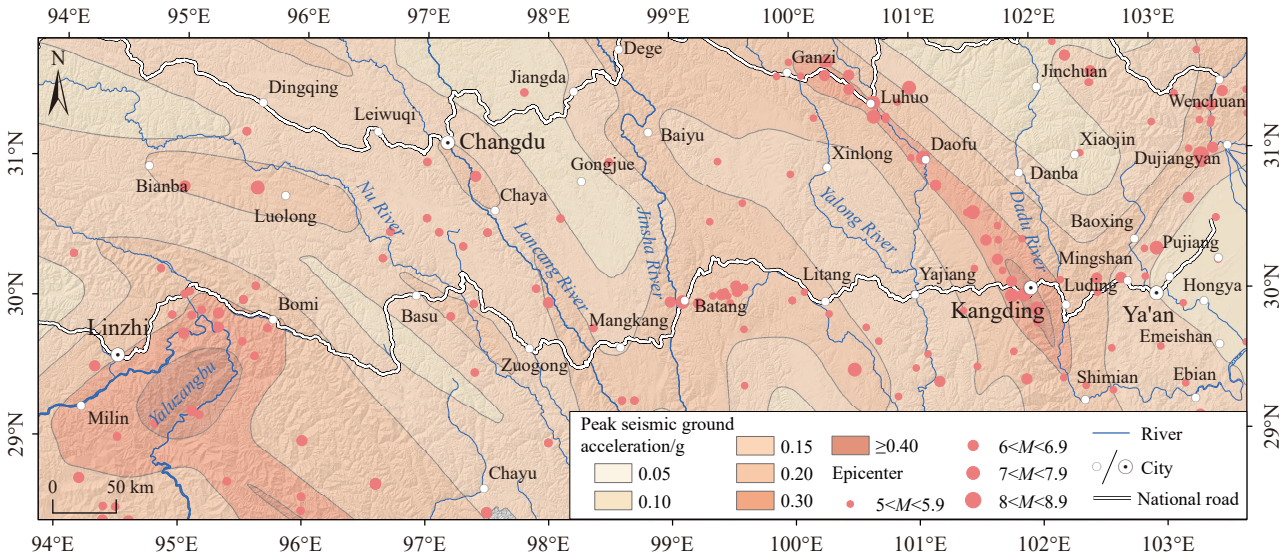

Fig. 9. Peak seismic ground acceleration in the Ya'an-Linzhi section of the Sichuan-Tibet transportation corridor.

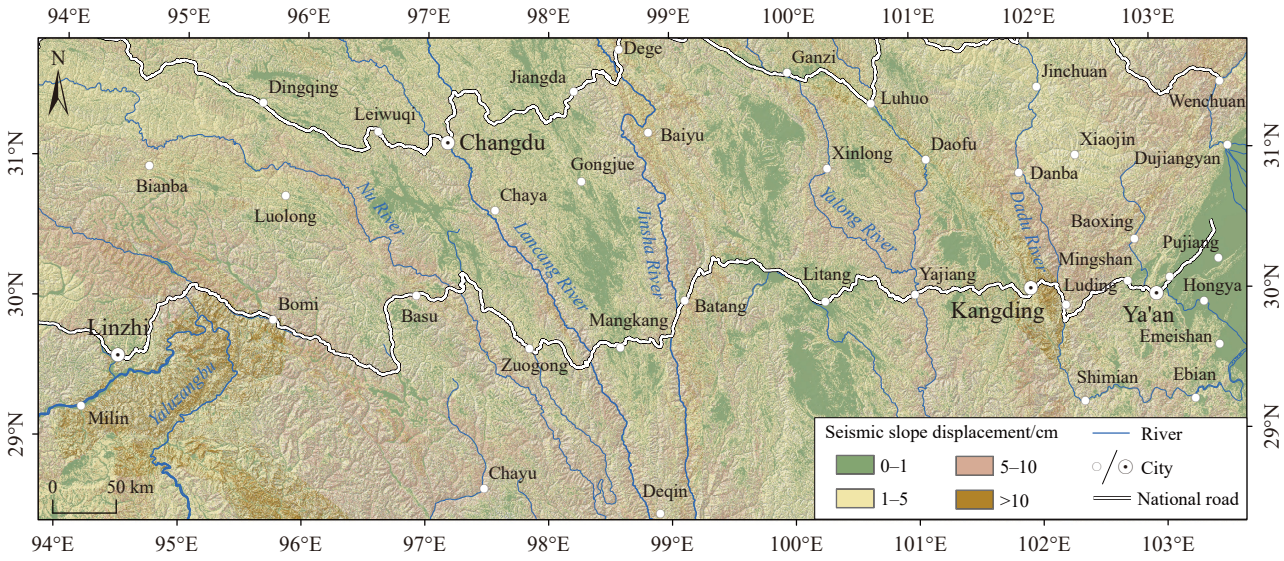

Fig. 10. Seismic slope displacement distribution in the Ya'an-Linzhi section of the Sichuan-Tibet transportation corridor.

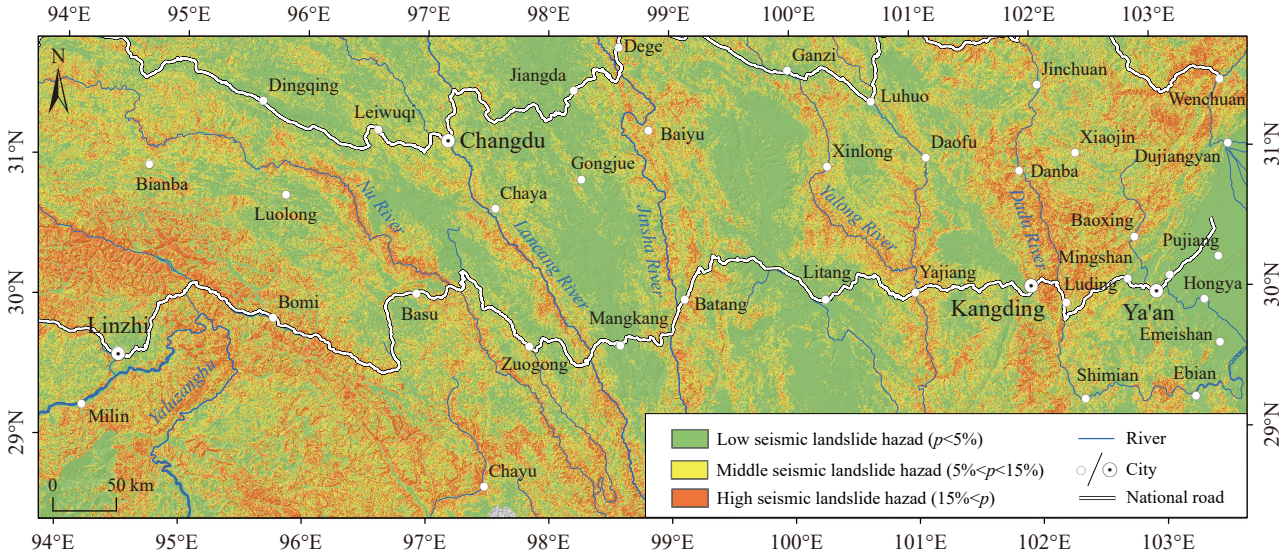

Fig. 11. Potential seismic landslide hazard in the Ya'an-Linzhi section of the Sichuan-Tibet transportation corridor.

where there are high seismic landslide hazard. The areas with low seismic landslide hazard are mainly distributed in the areas with gentle topography and little active tectonic effect, such as the Quaternary basins, broad river valleys and plateau planation planes.

5.2. Engineering effect of seismic landslide hazard

The statistical spatial distribution law of potential seismic landslide hazard shows that the major linear projects such as east-west railway, highway, water transmission line and trans-regional power grid in the Ya'an-Linzhi section of the Sichuan-Tibet transportation corridor mainly pass through five areas with high seismic landslide hazard. The first area is the Luding-Kangding section that is located at the Xianshuihe active fault zone, where the peak ground motion acceleration is up to 0.2–0.4 g, and the seismic risk is high, and the historical seismic landslides are developed. There have been many river blocking events resulting from seismic landslides and causing serious chain disasters. For example, the Mogangliang landslide with sliding body of 1.5×10^8 m^3 in the Luding county induced by the M_S $7^3/_4$ Kangding earthquake in 1876, resulted in blocking the Dadu river and forming a barrier lake with backwater length of 30 km and water storage of 13×10^8 m^3 (Zhao B et al., 2021). The second area is the Yajiang-Xinlong (Yalong River) section with peak ground motion acceleration of 0.15 g and relatively high seismic risk. The third area is the Batang-Baiyu (Jinsha river) section that is located at the Jinshajiang fault zone, with peak ground motion acceleration of 0.15–0.2 g and relatively high seismic risk and developed historical seismic landslides. These historical seismic landslides have resulted in many river blocking events, such as the earthquake-induced Temi landslide in the Batang county, which blocked the Jinsha river and formed big barrier lake, and the barrier dam remains till now. The fourth area is the Basu (Nujiang river) section that is located at the Nujiang fault zone, with the peak ground motion acceleration of 0.15 g, and high seismic risk. The fifth area is the Bomi-Linzhi (eastern Himalaya syntaxis) section that is located at the Jiali-Chayu active fault zone, with the peak ground motion acceleration of 0.2–0.3 g, and high seismic risk. Where, except for general landslides, the earthquake can also induce other geo-hazard with high risk, such as glacial lake outburst, glacial clastic flow.

The planned water transmission line (from the south to the north of China) in the study area mainly passes through the Batang-Baiyu (Jinsha river) section and Yajiang-Xinlong section with high seismic landslide hazard. A large number of tunnels and bridges of linear projects have been planned and deployed in the mountainous canyon area. And, the seismic landslides mainly pose potential threats to tunnel entrance and exit, bridge, roadbed, and other facilities. For example, the Dadu river bridge, Jinsha river bridge and Nujiang river bridge of a major line project are all under the potential threat of strong earthquake-induced collapse or landslide.

The point projects in the study area are mainly hydropower stations and mines. The hydropower stations are mainly planned and deployed along large rivers, such as the cascade hydropower station of Dadu river and Jinsha river, where are just the areas with high seismic landslide frequency. For example, the Batang hydropower station (the Temi landslide is in its reservoir area) and Suwalong hydropower station (the Xuelongnang landslide is in its reservoir area) are all under the potential of strong earthquake-induced landslide blocking river and surge disaster chain. Attention should be paid to the potential threat of seismic landslides to dams, factories, and other facilities.

6. Discussion

It is difficult to distinguish in detail the geo-hazard types induced by the different trigger factors such as rainfall,

earthquake, or human engineering activities. So, it is extremely difficult to obtain the detailed seismic landslide catalogue in a large area. The new or recent seismic geo-hazards are easy to investigate and record, but the historical seismic geo-hazards are difficult to identify accurately. The geo-hazards data in Fig. 3 include all the geo-hazards triggered by internal and external dynamic effects such as earthquake, rainfall, or human engineering activities. As present, the seismic geo-hazard data mainly include the local seismic geo-hazard since historical records, such as the geo-hazards induced by the Luhuo earthquake in 1973 and Luding earthquake in 2022 in the Xianshuihe fault zone, as well as typical historical seismic geo-hazards with well-preserved morphological signs.

The simplified Newmark model based on abundant statistical rules was adopted to complete this study. In view of the limitations of the Newmark model parameters, based on the landslide data induced by the M_S 7.9 Luhuo earthquake in the Xianshuihe fault zone in 1973, the localized Newmark model parameters adapted to the eastern Tibetan Plateau active fault zone were obtained, and the potential deterministic seismic landslide hazard assessment of the Xianshuihe fault zone was completed, and meaningful results were obtained (Zhang YS et al., 2017). So, this paper uses the presented Newmark model parameters to complete the calculation.

The presented study results generally reflect the spatial distribution law of regional potential probability seismic landslide hazard, which is basically consistent with field investigation and empirical understanding. However, the detailed seismic landslide catalogue within a big study area is fragmentary or lacking, and the geo-hazard data from single strong earthquake event is not suitable for the verification of the prediction results of probabilistic seismic landslide hazard. So, it is quite difficult to verify the prediction results of potential probabilistic seismic landslide hazard. Here, the relationship between typical large-scale historical seismic landslides (the Mogangling landslide, 55 Daoban landslide, Luanshibao landslide, Temi landslide, Wangdalong landslide, Langduo landslide group, Duolasi landslide and Jiaobunong landslide) in the region and the presented results is analyzed statistically. Most of these landslides are located at the areas with high seismic landslide hazard. The presented results are predictive and need to be further verified by the earthquake-induced landslide in the future.

Based on the above discussions, it is necessary to further optimize and obtain the localized Newmark model parameters, and establish the regional seismic landslide database to effectively promote the study on seismic landslide hazard and results verification, and further analyze the impact of seismic landslide hazard on the major project planning and construction, especially the key project sites.

7. Conclusions

The developed landslides have seriously restricted the planning and construction of major projects and social and economic activities in the Ya'an-Linzhi section of Sichuan-Tibet transportation corridor. For the long-term regional seismic landslide prevention and early control, the potential seismic landslide hazard assessment with a 50-year beyond probability 10% was completed. The main conclusions are as follows.

(i) The Sichuan-Tibet transportation corridor passes through several Holocene active faults, and many seismic landslide events have occurred in the history and in recent years. The sliding direction of seismic landslides is mostly perpendicular to the fault strike and the river flow direction, which is significantly controlled by the tectonics. The seismic landslides in the mountainous canyon areas are affected by the throwing force, with the characteristics of fast startup, large gravitational potential energy, long runout, and may be transformed into serious geo-hazard chain.

(ii) In general, the areas with high seismic landslide hazard are mainly distributed along large active tectonic belts and deep valleys of large rivers, which are significantly affected by tectonic activities. The areas with low seismic landslide hazard are mainly distributed in the areas with gentle topography and little active tectonic effect, such as the Quaternary basins, broad river valleys and plateau planation planes.

(iii) The major linear projects with east-west orientation in the Ya'an-Linzhi section of the Sichuan-Tibet transportation corridor mainly pass through five areas with high seismic landslide hazard: the Luding-Kangding section, the Yajiang-Xinlong (Yalong river) section, the Batang-Baiyu (Jinsha river) section, the Basu (Nujiang river) section, the Bomi-Linzhi (eastern Himalaya syntaxis) section. A large number of tunnels and bridges of linear projects have been planned and deployed in the mountainous canyon area. And, the seismic landslides mainly pose potential threats to tunnel entrance and exit, bridge, roadbed and other facilities.

(iv) Although presented study results can generally reflect the spatial distribution law of regional potential probability seismic landslide hazard, it is quite difficult to verify their accuracy in detail due to lack or incompleteness of the detailed seismic landslide catalogue within a big study area. In the future, the localized Newmark model need to be further optimized, and the regional seismic landslide database need to be established and completed for effectively promoting results accuracy.

CRediT authorship contribution statement

Zhi-hua Yang, Chang-bao Guo and Rui-an Wu conceived of the presented idea. Zhi-hua Yang, Wei-wei Shao, Peng-fei Yu and Cai-hong Li carried out the analysis and calculation. All authors participated in the field survey and discussed the results and contributed to the final manuscript.

Declaration of competing interest

The authors declare no conflicts of interest.

Acknowledgements

This research was supported by the National Natural Science Foundation of China (42277180), China Geological Survey Project (DD20221816), National Key Research and Development Program of China (2021YFB2301403-5) and State Key Laboratory of Resources and Environmental Information System.

References

Chousianitis K, Del Gaudio V, Kalogeras I, Ganas A. 2014. Predictive model of Arias intensity and Newmark displacement for regional scale evaluation of earthquake-induced landslide hazard in Greece. Soil Dynamics and Earthquake Engineering, 65, 11–29. doi: 10.1016/j.soildyn.2014.05.009.

Dai FC, Xu C, Yao X, Xu L, Tu XB, Gong QM. 2011. Spatial distribution of landslides triggered by the 2008 M_S 8.0 Wenchuan earthquake, China. Journal of Asian Earth Sciences, 40(4), 883–895. doi: 10.1016/j.jseaes.2010.04.010.

Delaney KB, Evans SG. 2015. The 2000 Yigong landslide (Tibetan Plateau), rockslide-dammed lake and outburst flood: Review, remote sensing analysis, and process modelling. Geomorphology, 246, 377–393. doi: 10.1016/j.geomorph.2015.06.020.

Deng QD. 1996. Active Tectonics in China. Geological Review, 42(4), 295–299. doi: 10.16509/j.georeview.1996.04.003.

Du GL, Zhang YS, Zou L, Yang ZH, Yuan Y, Ren SS. 2022. Co-seismic landslide hazard assessment of the 2017 M_S 6.9 Milin earthquake, Tibet, China, combining the logistic regression –information value and Newmark displacement models. Bulletin of Engineering Geology and the Environment, 81, 446. doi: 10.1007/s10064-022-02901-x.

Fan XM, Wang X, Dai LX. 2022. Characteristics and spatial distribution pattern of M_S 6.8 Luding Earthquake occurred on September 5, 2022. Journal of Engineering Geology, 30(5), 1504-1516 (in Chinse with English abstract). doi: 10.13544/j.cnki.jeg.2022-0665.

Guo CB, Zhang YS, Montgomery DR, Du YB, Zhang GZ, Wang SF. 2016. How unusual is the long-runout of the earthquake-triggered giant Luanshibao landslide, Tibetan Plateau, China? Geomorphology, 259, 145–154. doi: 10.1016/j.geomorph.2016.02.013.

Guo CB, Montgomery DR, Zhang YS, Zhong N, Fan C, Wu RA, Yang ZH, Ding YY, Jin JJ, Yan YQ. 2020. Evidence for repeated failure of the giant Yigong landslide on the edge of the Tibetan Plateau. Scientific Reports, 10, 14371. doi: 10.1038/s41598-020-71335-w.

Hua JX, Zheng JG, Wang DL. 2018. Engineering Geology Handbook (Fifth edition) of China. China Architecture and Building Press, Beijing (in Chinese).

Huang YD, Xie CC, Li T, Xu C, He XL, Shao XY, Xu XW, Zhan T, Chen ZN. 2022. An open-accessed inventory of landslides triggered by the M_S 6.8 Luding earthquake, China on September 5, 2022. Earthquake Research Advances, 3(1), 100181. doi: 10.1016/j.eqrea.2022.100181.

Jibson RW. 1993. Predicting earthquake-induced landslide displacements using Newmark's sliding block analysis. Transportation Research Record, 1411, 9–17.

Jibson RW, Harp EL, Michael JA. 2000. A method for producing digital probabilistic seismic landslide hazard maps. Engineering Geology, 58(3–4), 271–289. doi: 10.1016/S0013-7952(00)00039-9.

Jibson RW. 2007. Regression models for estimating coseismic landslide displacement. Engineering Geology, 91(2 –3), 209 –218. doi: 10.1016/j.enggeo.2007.01.013.

Kamp U, Growley BJ, Khattak GA, Owen LA. 2008. GIS based landslide susceptibility mapping for the 2005 Kashmir earthquake region. Geomorphology, 101(4), 631–642. doi: 10.16738/j.cnki.issn.1003-3238.2012.04.007.

Lee S, Evangelista DG. 2006. Earthquake-induced landslide-susceptibility mapping using an artificial neural network. Natural Hazards and Earth System Science, 6(5), 687–695. doi: 10.5194/nhess-6-687-2006,2006.

Li MH, Wang DH, Gao YC, Bai YJ. 2014. Research on the Geohazards Induced by the M7. 9 Luhuo Earthquake in Xianshuihe Fault Zone. Journal of Catastrophology, 29(1), 37–41.

Li C, Su LJ. 2021. Influence of critical acceleration model on assessments of potential earthquake –induced landslide hazards in Shimian County, Sichuan Province, China. Landslides, 18(5), 1659–1674. doi: 10.1007/s10346-020-01578-1.

Meng W, Guo CB, Zhang YS, Du YB, Zhang M, Bao LH, Zhang P. 2022. In situ stress measurements in the Lhasa terrane, Tibetan Plateau, China. Acta Geologica Sinica (English Edition), 90(6), 2022–2035. doi: 10.1111/1755-6724.13019.

Miles SB, Ho CL. 1999. Rigorous landslide hazard zonation using Newmark ’s method and stochastic ground motion simulation. Soil Dynamics and Earthquake Engineering, 18, 305–323. doi: 10.1016/S0267-7261(98)00048-7.

Nefeslioglu HA, Duman TY, Durmaz S. 2006. Landslide susceptibility mapping for a part of tectonic Kelkit Valley (Eastern Black Sea region of Turkey). Geomorphology, 94(3–4), 401–418. doi: 10.1016/j.geomorph.2006.10.036.

Newmark NM. 1965. Effects of earthquakes on dams and embankments. Geotechnique, 15(2), 139–160. doi: 10.1680/geot.1965.15.2.139.

Nowicki MA, Wald DJ, Hamburger MW, Hearne M, Thompson EM. 2014. Development of a globally applicable model for near real-time prediction of seismically induced landslides. Engineering Geology, 173, 54–65. doi: 10.1016/j.enggeo.2014.02.002.

Peng C, Yin ZQ, Zhang XJ, Shao H, Pang MF. 2021. A comparative study of the main factors controlling geohazards induced by seismic events in Western China since the Wenchuan earthquake. China Geology, 5, 1–15. doi: 10.31035/cg2022009.

Roberto R. 2000. Seismically induced landslide displacements: a predictive model. Engineering Geology, 58(3 –4), 337 –351. doi: 10.1016/S0013-7952(00)00042-9.

Shao XY, Xu C, Ma SY. 2022. Preliminary Analysis of Coseismic Landslides Induced by the 1 June 2022 M_S 6.1 Lushan Earthquake, China. Sustainability, 14(24), 16554. doi: 10.3390/su142416554.

Song YQ, Gong JH, Gao S, Wang DC, Cui TJ, Li Y, Wei BQ. 2012. Susceptibility assessment of earthquake-induced landslides using Bayesian network: A case study in Beichuan, China. Computers & Geosciences, 42, 189–199. doi: 10.1016/j.cageo.2011.09.011.

Tang HM, Liu X, Hu XL, Griffiths DV. 2015. Evaluation of landslide mechanisms characterized by high-speed mass ejection and long-run-out based on events following the Wenchuan earthquake. Engineering Geology, 194, 12–24. doi: 10.1016/j.enggeo.2015.01.004.

Tapponnier P, Molnar P. 1977. Active faulting and tectonics in China.

Journal of Geophysical Research, 82, 2905–2930. doi: 10.1029/JB082i020p02905.

The Ministry of Construction of the People's Republic of China. 2010. National Standard of the People's Republic of China "Code for Seismic Design of Buildings" (GB 50011-2010). China Architecture and Building Press, Beijing (in Chinese).

Wang T, Wu SR, Shi JS, Xin P. 2013. Application and Validation of Seismic Landslide Displacement Analysis Based on Newmark Model: A Case Study in Wenchuan Earthquake. Acta Geologica Sinica (English Edition), 87(supp.), 393–397.

Wang T, Wu SR, Shi JS, Xin P, Wu LZ. 2018. Assessment of the effects of historical strong earthquakes on large-scale landslide groupings in the Wei River midstream. Engineering Geology, 235, 11–19. doi: 10.1016/j.enggeo.2018.01.020.

Wilson RC, Keefer DK. 1983. Dynamic analysis of a slope failure from the 6 August 1979 Coyote lake, California, earthquake. Bulletin of Engineering Geology and the Environment, 73(3), 863–877. doi: 10.1016/0040-1951(84)90122-7.

Wu RA, Zhang YS, Guo CB, Yang ZH, Su FR, Tang J. 2020. Landslide susceptibility assessment in mountainous area: a case study of Sichuan-Tibet railway, China. Environmental Earth Sciences, 79, 157. doi: 10.1007/s12665-020-8878-8.

Xu C, Dai FC, Xu XW, Lee YH. 2012. GIS-based support vector machine modeling of earthquake-triggered landslide susceptibility in the Jianjiang River watershed, China. Geomorphology, 145 –146, 70–80. doi: 10.1016/j.geomorph.2011.12.040.

Yang ZH, Lan HX, Gao X, Li LP, Meng YS, Wu YM. 2015. Urgent Landslide Susceptibility Assessment in the 2013 Lushan Earthquake-impacted Area, Sichuan Province, China. Natural Hazards, 75(3), 2467–2487. doi: 10.1007/s11069-014-1441-8.

Yin YP, Zheng WM, Li XC, Sun P, Li B. 2011. Catastrophic landslides associated with the M_S 8. 0 Wenchuan earthquake. Bulletin of Engineering Geology and the Environment, 70(1), 15–32. doi: 10.1007/s10064-010-0334-7.

Yin YP. 2014. Vertical acceleration effect on landsides triggered by the Wenchuan earthquake, China. Environmental Earth Sciences, 71, 4703–4714. doi: 10.1007/s12665-013-2860-7.

Zhang YS, Dong SW, Hou CT, Guo CB, Yao X, Li B, Du JJ, Zhang JG. 2013. Geohazards induced by the Lushan M_S 7.0 earthquake in Sichuan Province, Southwest China: typical examples, types and distributional characteristics. Acta Geologica Sinica (English Edition), 87(3), 646–657. doi: 10.1111/1755-6724.12076.

Zhang YS, Yang ZH, Guo CB, Wang T, Wang DH, Du GL. 2017. Predicting landslide scenes under potential earthquake scenarios in the Xianshuihe fault zone, Southwest China. Journal of Mountain Science, 14(7), 1262–1278. doi: 10.1007/s11629-017-4363-6.

Zhao B, Wang YS, Wu JF, Su LJ, Liu JW, Jin G. 2021. The Mogangling giant landslide triggered by the 1786 Moxi M 7.75 earthquake, China. Natural Hazards, 106, 459 –485. doi: 10.1007/s11069-020-04471-1.

Zhu SB, Shi YL. 2005. Genetic Algorithm-Finite Element Inversion of Topographic Spreading Forces and Drag Forces of Lower Crust to Upper Crust in Tibetan Platea. Acta Scientiarum Naturalium Universitatis Pekinensis, 41(2), 225–234. doi: 10.13209/j.0479-8023.2005.030.